Modeling High-current Relativistic Beams in Ray-tracing Codes

Stanley Humphries
Field Precision

and

John Petillo
Science Applications International Corporation

Abstract

1. Introduction

This paper describes a new method to calculate beam-generated magnetic fields in two-dimensional ray-tracing codes. The technique is useful for modeling high-current relativistic electron beams where the magnetic force is comparable to the electrical force arising from space charge. The discussion concentrates on the application to cylindrical beams in finite-element codes employing conformal triangular meshes for the electric field calculation[1-4]. The extension to codes with box meshes[5-9] is straightforward. The approach is based on the assignment of model particle currents to the faces of elements on the same mesh used for the electrostatic calculation. We then derive enclosed currents and values of toroidal field at mesh vertices by tracing a logical path along faces to the axis. The technique has several advantages:

- Field interpolations are more accurate than those on a simple rectangular mesh.

- Use of the same mesh and interpolation method reduces systematic differences in calculations of electric and magnetic forces. The balanced calculations are resistant to numerical filamentation instabilities in highly-relativsitic beams.

- Implementation of the magnetic calculation requires little extra run time because the main tasks of identifying elements along particle trajectories and collecting interpolation points are already performed for the electric field calculation.

- Because element faces in the mesh conform to the surfaces of materials, orbit intersections with surface faces can be used to find the distribution of current on source and collector electrodes. The toroidal magnetic fields produced by feed currents can strongly influence the dynamics of beams from convex emitters.

Section 2 reviews the ray-tracing technique and previous appoaches to the calculation of beam-generated magnetic forces. Section 3 describes the assignment of model particle currents to element faces, the basis of our procedure. The method automatically satisfies the condition $\nabla \cdot \boldsymbol{j} = 0$ in the beam propagation region and gives the correct distribution of surface currents on electrodes. The algorithm is tolerant to variations in element size and time step and correctly accounts for reflex orbits. Section 4 covers the conversion of face currents into values of toroidal field. Balanced current and space-charge averaging can be introduced to eliminate oscillations of field quantities between iteration cycles. Finally, Section 5 describes benchmark calculations performed with the ETrak code to illustrate the accuracy and versatility of the method.

2. Ray tracing method

Ray-tracing is a familiar technique[10] to find self-consistent steady-state electric fields in high-current charged-particle guns. A variety of finite-difference and finite-element codes[1-9] have been developed in the last two decades. Figure 1 illustrates the mesh used for cylindrical finite-element solutions in ETrak. The triangles are the cross-sections of small volumes that are figures of revolution about the axis. We shall refer to the volumes as *elements*, the surfaces of the elements as *faces*, and the intersection of the faces as *vertices*. ETrak uses a structured conformal mesh with vertices organized in columns (index i along the z direction) and rows (index j along the r direction). The ray-tracing procedure for non-relativistic beams starts from a vacuum electrostatic solution consisting of values of potential $\varphi(i,j)$ at vertices. The code generates several model particles (denoted by indices $1 \le n \le N$) to represent the beam. Each particle carries a portion I_n of the beam current. (Note that I_n has a negative value for electrons.)

The sum of model particle currents equals the full beam current I:

$$I = \sum_{n=1}^{N} I_n. \qquad \textbf{(1)}$$

The values of I_n and the initial positions and momenta of model particles may be specified to represent an incident beam. Alternatively, the quantities may be determined by the code from the source geometry and a local application of a Child law emission algorithm[4]. The program tracks each particle in turn, numerically integrating the equations of motion over time step Δt using local interpolations for the electric field. For each model particle the process yields a set of differential orbit vectors, $\boldsymbol{X}_{pk}$ in the (r,z) solution space. The initial and final positions of a particle are given by

$$\boldsymbol{X}_{pf} = \boldsymbol{X}_{pi} + \sum_{k} \boldsymbol{X}_{pk}. \qquad \textbf{(2)}$$

To assign space charge the program determines the element that contains the midpoint of $\boldsymbol{X}_{pk}$ and increments the element charge by $I_n \Delta t$. After tracking all particles the program recalculates the electrostatic field with the added space-charge and then retraces the orbits. The process repeats

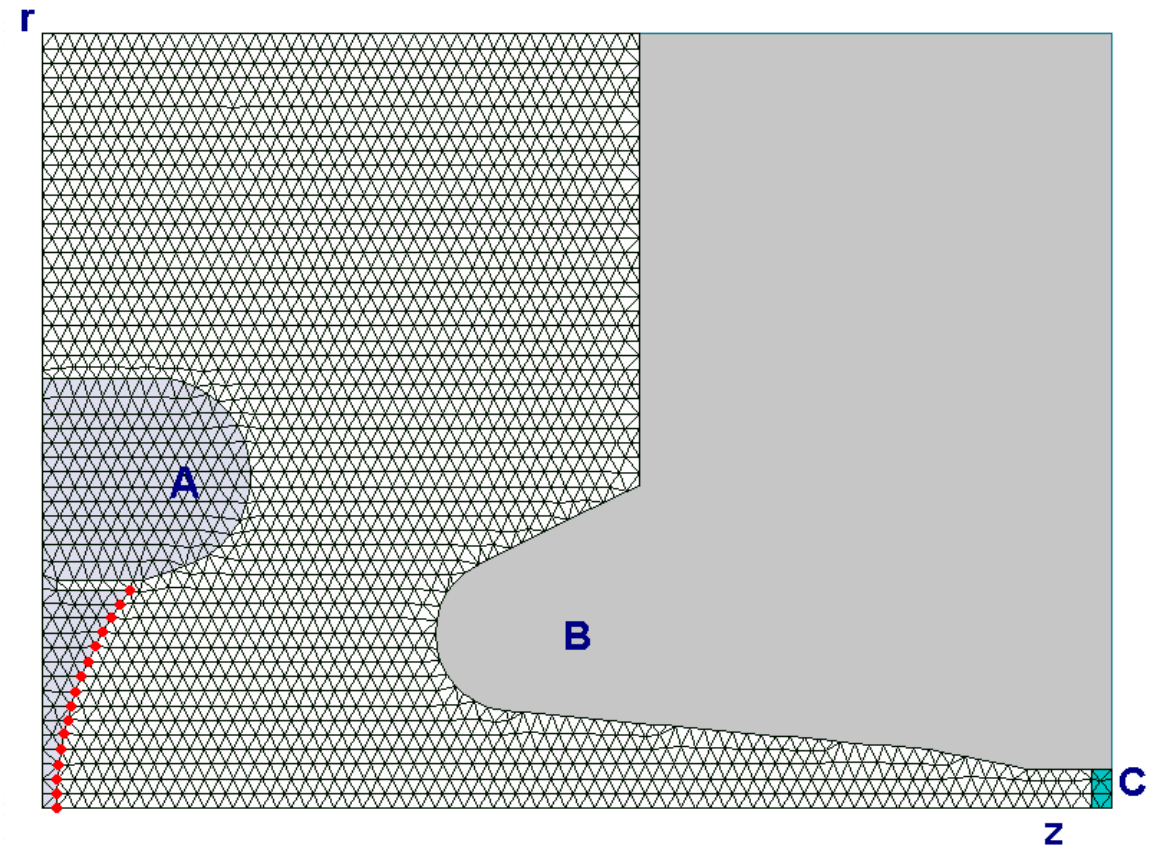

Figure 1. Conformal triangular mesh for a cylindrical high-current electron gun. The triangles are the cross-sections of elements. The sides of the triangles are faces and the intersections of faces are vertices. The blue triangles (A) constitute a region constant potential elements to represent the cathode and focusing electrode. The vertices marked in red act as sources points and the connecting lines are Emission faces. The lines that constitute the surface of the anode (B) are Collector faces. The green Material region marked C is a target to stop electrons.

for several cycles. With suitable space-charge averaging between cycles, the technique usually converges to a self-consistent solution.

For relativistic beams a ray-tracing code must also find the distribution of beam current to calculate magnetic forces. Although the mathematical expression for magnetic fields in cylindrical systems is simple, development of a procedure that can handle all practical cases is challenging. One approach used in several codes is *ray counting*. If the presently-tracked particle is at position (r_n,z_n), then the code determines all rays that have smaller radius at z_n. The enclosed axial current I_{ez} equals the sum of internal ray currents plus one-half that of the present ray,

$$I_{ez} = \sum_{r_n' < r_n} I_n' + \frac{I_n}{2}. \qquad \textbf{(3)}$$

The toroidal field is related to the enclosed current by

$$B_\theta(r,z) = \mu_o \frac{I_{ez}}{2\pi r}. \quad \textbf{(4)}$$

In a code that tracks rays sequentially, the ray-counting method is useful only for laminar beams. In this case the particles maintain their radial order, and the enclosed currents are invariant. The process becomes unwieldy for beams with non-zero emittance where the radial order changes with *z*. Alternatively, a code can advance all model particles simultaneously, but the calculation of I_{ez} is straightforward only when particles move with about the same axial velocity (*paraxial* motion). The main problem with ray counting is that electric forces are determined from the particle distribution on the previous iteration cycle while the magnetic forces depend on the present distribution. The imbalance may inhibit convergence of high-current solutions. Furthermore, ray counting is not well-suited to the treatment of reflex orbits or counter-streaming flows.

Another option that we have used in the Trak code[3,4] is first to accumulate the current of each ray on a simple independent mesh, next to determine values of enclosed current and B_θ, and finally to use interpolations to find the magnetic force on particles in the following iteration cycle. This approach handles non-laminar and non-paraxial beams and resolves the problem of cycle offsets. Nonetheless, the method has two drawbacks. For highly relativistic beams small systematic differences in interpolations on the electric and magnetic meshes may cause a numerical instability where the beam separates radially into filaments. Furthermore, a simple magnetic mesh yields poor interpolations near curved emission surfaces.

Sometimes, the problems of filamentation and non-laminar beams can be resolved by tracking orbits in the *relativistic mode*. The approach is simply to omit the magnetic force calculation and to divide the transverse electric field force by $1/\gamma^2$. Here, the quantity γ is the radially-averaged relativistic energy factor of the beam. The approximation holds only under two circumstances: 1) particle motion is paraxial and 2) the transverse electric arises solely from the beam space-charge. The relativistic mode is not valid in electron guns or acceleration gaps. A further drawback is that the code user must decide when to switch modes, increasing the chances for non-physical results. The method we describe in the following sections has the advantages of the mesh approach and resolves the problems of surface interpolations. Furthermore, the accuracy of the balanced calculations of electric and magnetic forces make it unnecessary to invoke the relativistic mode.

3. Current assignment to element faces

In order to understand current assignment on a triangular mesh, it is useful to review briefly how self-consistent non-relativistic orbits are determined in ETrak from electric field information. Figure 1 shows the conformal mesh used to calculate electrostatic potential in a high-current gun. In ETrak contiguous elements and vertices with the same material properties are called *regions* and are marked with a region number. In the electrostatic calculation, regions are assigned physical properties to represent electrodes, dielectrics, vacuum volumes or fixed-potential

boundaries. For orbit tracking, regions are divided into three classes: 1) *Vacuum*, 2) *Material* and 3) *Secondary*. Particles move through Vacuum elements and stop if they enter a Material element. A collision with a Secondary element results in re-emission of an electron. Secondary materials are discussed in a separate paper[11].

An ETrak simulation of a non-relativistic gun without secondary electrons consists of the following operations:

- Find a vacuum electrostatic solution and (optionally) an *applied* magnetic field solution on an independent mesh.

- Initiate model particles near an emission surface and assign currents I_n.

- Integrate the relativistic equations of motion for each particle sequentially by a time-centered method[12] with step Δt. During this process, the code must identify elements that contain the ends and midpoint of the particle orbit vectors $\boldsymbol{X}_{pk}$ to perform electric field interpolations.

- For each time step increment the space charge in the element at the midpoint by $I_n \Delta t$.

- Stop the particles if they leave the solution volume or enter a Material element.

- Recalculate the field using the space-charge distribution generated by the full set of model particle traces.

- Repeat the process for several cycles to achieve convergence.

Current assignment for the beam-generated magnetic field calculation is performed during orbit integrations at the same time as space-charge assignment. The process employs the available information on which element contains the orbit vector. The main difference is that particle currents are assigned to element faces rather than volumes to ensure conservation of current. We shall concentrate on general features of the method - the detailed index operations are laborious even on a structured triangular mesh. Suppose that given a location (r,z) we can identify the occupied element, the vertices and faces of the element, and the neighboring elements. Furthermore, the code can find the nature of the face, one of four types:

- *Interior* faces have Material or Secondary elements on both sides. These faces are inside electrodes. They do not contribute to the magnetic field solution.

- *Vacuum* faces have Vacuum elements on both sides. This type of face fills the beam propagation volume.

- *Emission* faces connect vertices that define the emission (or source) surface. Particles enter the solution volume through Emission faces. Reflex orbits may also leave through an Emission face.

• *Collector* faces have a Vacuum element on one side and a Material or Secondary element on the other. All faces on electrode surfaces that are not Emission faces are Collector faces. Particles leave the solution volume through Collector faces.

To begin, consider the treatment of Vacuum faces. Suppose that during the orbit integration for particle *n* the program detects that the ends of a particle vector $\boldsymbol{X}_{pk}$ lie in adjacent vacuum elements (Fig. 2). In this case, the particle has crossed the intervening Vacuum face. We form a surface vector $\boldsymbol{X}_s$ from the face end points arranged so that the vector points radially outward. If the cross product $\boldsymbol{X}_{pk} \times \boldsymbol{X}_s$ is positive, the particle has crossed toward higher values of *z* and we increment the face current by $+I_n$. If the cross-product is negative, the current is adjusted by $-I_n$.

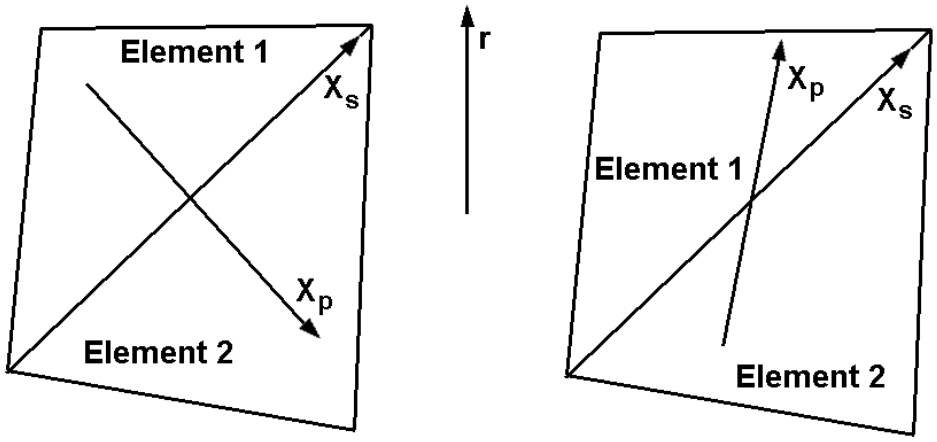

Figure 2. Particles crossing a shared face between adjacent elements. Definition of the particle vector $\mathbf{X}_p$ and surface vector $\mathbf{X}_s$. The cross product $\mathbf{X}_p \times \mathbf{X}_s$ is positive in the case on shown on the left and negative for the case on the right.

A particle that crosses a Collector face leaves the solution volume and contributes to current flow on the electrode surface. Therefore, the current of a Collector face is always incremented by $+I_n$, regardless of the direction of the orbit vector. The following section shows that this convention yields the correct values of I_{ez} for electrodes of any shape as long all surface vertices logically connect to the axes along a path of Collector faces. Emission faces are more involved because we want to include the possibility of reflected particles that may return to the source. At the beginning of the calculation, the program makes a record of all emission faces, checks that they constitute a contiguous surface logically-connected to the axis, and then arranges them in order starting at the axis (Fig. 3). When a particle with orbit vector $\boldsymbol{X}_{pk}$ crosses an emission face, the program creates a surface vector $\boldsymbol{X}_s$ from the end points of the face arranged so that the vector points away from the axis intersection. If the cross-product $\boldsymbol{X}_{pk} \times \boldsymbol{X}_s$ is positive, the particle is leaving the source and the program increments the face current by $+I_n$. A negative value of the cross product indicates that the particle has re-entered the source, and the current is changed by $-I_n$.

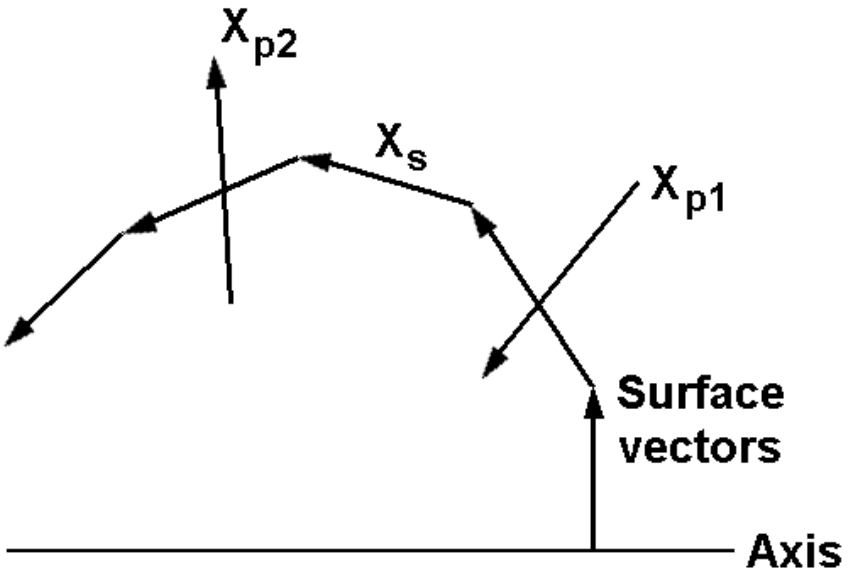

Figure 3. Assigning current to Emission faces. Particle 1 re-enters the source and the cross-product $\mathbf{X}_{p1} \times \mathbf{X}_s$ is negative. The cross product for a particle that exits the source (Particle 2) is positive.

On a conformal mesh we must anticipate that a particle may cross several elements in a time step in regions of high mesh resolution. In this case, the program makes a local search of faces near the midpoint of the orbit vector to check for intersections with $\boldsymbol{X}_{pk}$. The current of interesected faces is changed following the rules for Vacuum, Collector or Emission faces. Figure 4 illustrates a quick method to check intersections. The particle vector has the start point $\boldsymbol{X}_{p1} = (z_{p1},r_{p1})$ at t and end point $\boldsymbol{X}_{p2} = (z_{p2},r_{p2})$ at $t + \Delta t$. The element face is represented by the vectors $\boldsymbol{X}_{s1} = (z_{s1},r_{s1})$ and $\boldsymbol{X}_{s2} = (z_{s2},r_{s2})$. From the coordinates we form the following set of vectors:

$$\begin{aligned}
\boldsymbol{X}_{a3} &= \boldsymbol{X}_{p2} - \boldsymbol{X}_{p1}, \\
\boldsymbol{X}_{a1} &= \boldsymbol{X}_{s1} - \boldsymbol{X}_{p1}, \\
\boldsymbol{X}_{a2} &= \boldsymbol{X}_{s2} - \boldsymbol{X}_{p1}, \\
\boldsymbol{X}_{b3} &= \boldsymbol{X}_{s2} - \boldsymbol{X}_{s1}, \\
\boldsymbol{X}_{b1} &= \boldsymbol{X}_{p1} - \boldsymbol{X}_{s1}, \\
\boldsymbol{X}_{b2} &= \boldsymbol{X}_{p2} - \boldsymbol{X}_{s1}.
\end{aligned} \qquad \textbf{(5)}$$

An intersection occurs if the following two conditions are true.

• The cross products $\boldsymbol{X}_{a3} \times \boldsymbol{X}_{a1}$ and $\boldsymbol{X}_{a3} \times \boldsymbol{X}_{a2}$ point in opposite directions.

• The cross products $\boldsymbol{X}_{b3} \times \boldsymbol{X}_{b1}$ and $\boldsymbol{X}_{b3} \times \boldsymbol{X}_{b2}$ point in opposite directions.

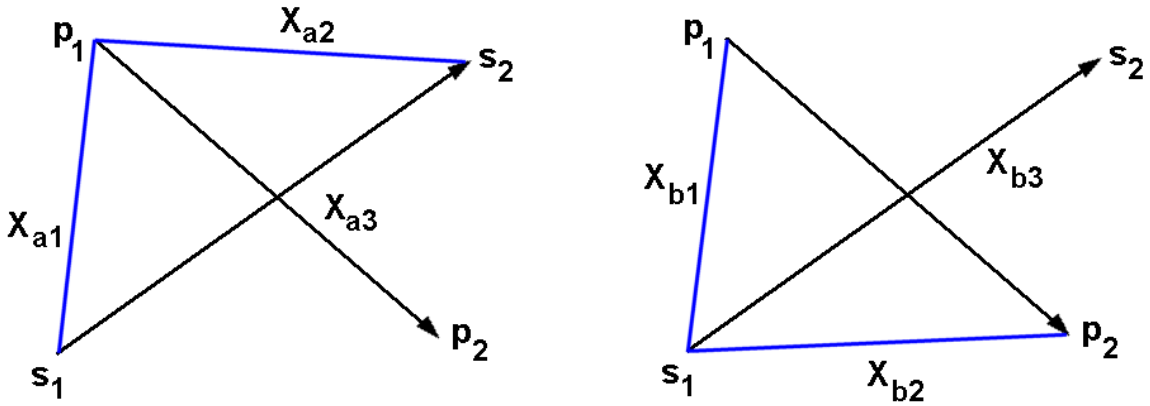

Figure 4. Vectors to check the intersection of a particle vector with a face vector.

To conclude this section, we mention some guidelines for assigning current to Collector and Emission faces in a practical code. It is essential to ensure that the currents of particles that leave the solution space are registered on the exit surface. The following rule applies to the two-step orbit integration method used in ETrak. If a particle enters a Material or Secondary element on either the full or half time step, current is assigned to an intersected Collector or Emitter face before the orbit is terminated. A second concern is that the current of entering particles is correctly assigned to Emission faces. The problem is that particles must be created in a vacuum element to guarantee a valid initial field interpolation. The method of resolution depends on which calculation mode is used for the ETrak run.

Track Mode. Particles are initiated from an externally-supplied list of parameters (position vector, momentum vector and current), possibly from a previous calculation.

Space-charge Limited Emission Mode. The program generates a set of particles for each vertex of the Emission surface based on a local application of the Child Law. The program creates the particles at a computational surface in vacuum close to the Emission surface.

In the Track Mode the particles are usually generated with specified current close to a boundary or electrode marked as an Emission surface. In this case, the program loops through the particles and assigns I_n to the closest Emission face. For the Space-charge Limited Emission mode ETrak uses a method to create particles and set currents that is particularly well-suited to the magnetic field calculation[4]. The program projects orbits backward from the computational surface to the

Emission surface before undertaking the standard integration in the forward direction. During reverse tracking the program assigns current to intersected Emission faces using the following rule: $-I_n$ if the cross-product $\boldsymbol{X}_{pk} \times \boldsymbol{X}_s$ is positive and $+I_n$ otherwise.

4. Converting face currents to enclosed current and toroidal magnetic field

When orbit integrations are complete the program converts face current information to a set of values of enclosed current I_{ez} on vertices and then to values of B_θ through Eq. 4. These values can then be used to find magnetic forces in the following cycle using linear or higher-order interpolations. The first step of the conversion process is to scan the mesh and to set a flag that marks all valid vertices as *Unprocessed*. Here the term *valid* indicates that the vertex is a part of at least one vacuum element. The next step is to set enclosed current on vertices connected to Emission or Collector faces. The program searches the bottom row of the mesh ($j = 1$) corresponding to the axis or minimum radius of the solution space. When a vertex connected to an Emission or Collector surface is located, the program sets $I_{ez} = 0$ and marks the point as *Processed*. It then checks whether the vertex is logically-connected to an Unprocessed Collector or Emission point. The program moves to the connected vertex and sets the enclosed current equal to that on the previous vertex plus the current of the connecting face. The process continues until there is no Unprocessed point connected along a Collector or Emission face. The program then searches for any other sets of surface points connected to the axis. Section 5 shows that the procedure correctly sets currents on feed electrodes, even with complex reentrant geometries.

The next step is to set included currents at the remaining valid points that fill the vacuum propagation volume. The program sets $I_{ez} = 0$ for remaining points on axis and marks them as Processed. It them moves radially outward row by row looking for Unprocessed points. For each vertex on row j, the program looks for a connection along a face to the Processed point on row $j-1$ with the smallest axial displacement. It then sets the enclosed current equal to that of the interior point plus that of the connecting face and marks the vertex as processed. If there are any Unprocessed points after reaching the top row, the program repeats the mesh scan.

It is essential to average beam charge and current between cycles to ensure stability of the ray-tracing procedure. For example, consider Child law space-charge assignment. On one cycle, the electric field near the cathode may be strong, resulting in the large particle currents on the following cycle. The resulting enhanced space-charge density suppresses fields near the cathode, giving low current on the following cycle. To prevent cycle-to-cycle oscillations it is usually necessary to make gradual corrections of the space charge by averaging with values from previous cycles. To preserve force balance in relativistic beams the same averaging should be applied to beam-generated magnetic fields. To implement averaging on cycle K we use the equation

$$B_\theta^K = \zeta \frac{\mu_o I_{ez}^{K-1}}{2\pi r} + (1-\zeta)\, B_\theta^{K-1}. \qquad \textbf{(6)}$$

In Eq. 6 the averaging constant ζ is in the range $0 < \zeta < 1$. Low values of ζ give small corrections averaged over many cycles.

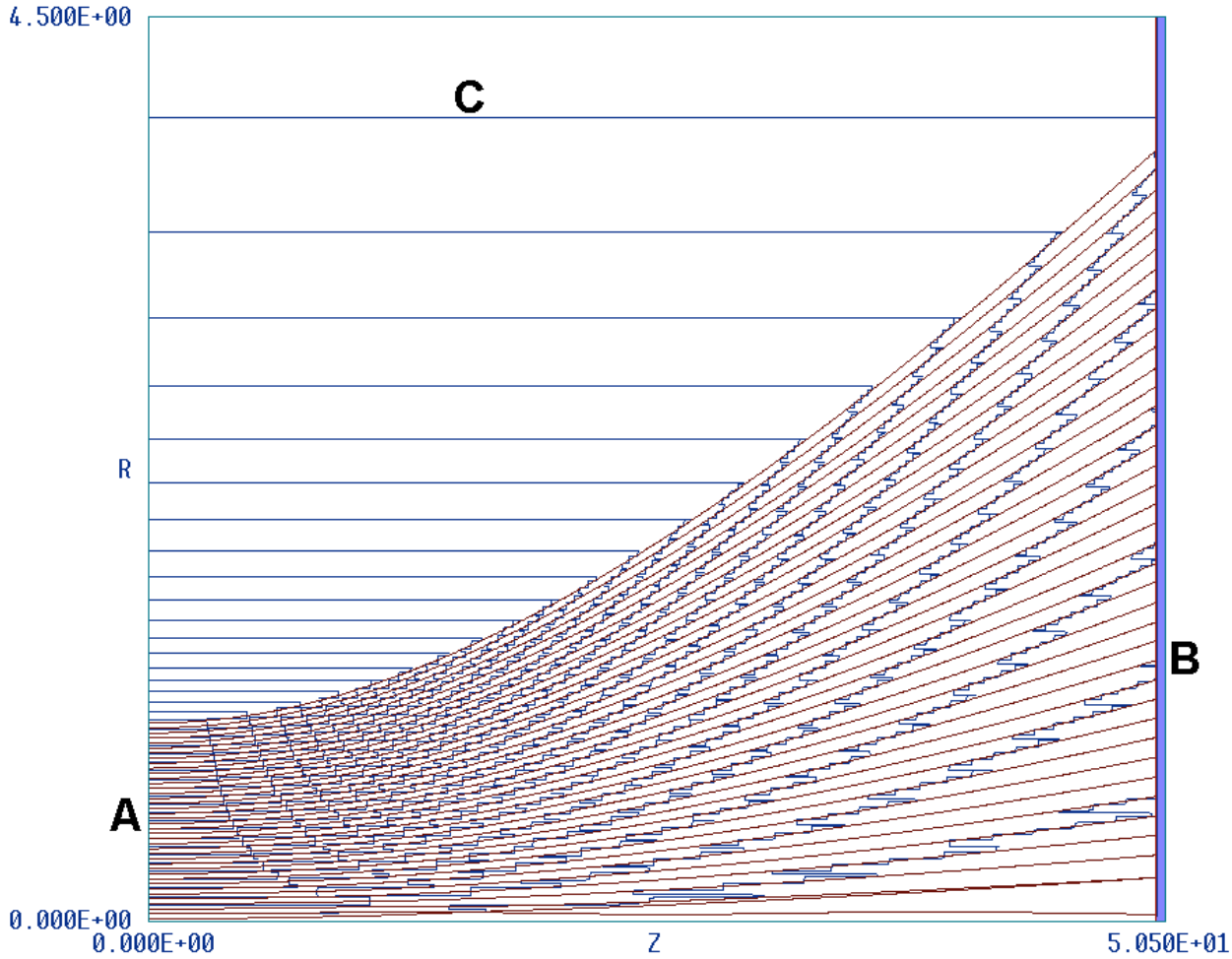

Figure 5. Expansion of a relativistic beam in free space: 617.4 A, 1 MeV. Particle orbits in black. Dimensions in cm. 10× vertical exaggeration. A) Emission surface. B) Target region with Collector surface. C) Contour lines of constant B_θ.

5. Benchmark calculations

This section covers several calculations that demonstrate the accuracy and validity of the face-current technique. Although the results look straightforward, they would be difficult to achieve with the methods reviewed in Sect. 2. To begin consider the expansion of a uniform-current-density relativistic electron beam in free space. The calculation is a sensitive test of accuracy because forces arise solely from the presence of the beam. In the example a 617.4 A beam with 1 MeV kinetic energy starts from a waist point with radius 1.0 cm. For a grounded wall radius of 3.0 cm the predicted[13] space-charge potential on axis at the waist is 62.93 kV. Therefore, we can assume that the kinetic energy changes little during expansion. The predicted beam expansion factor[13] for a 50 cm transport distance is $r_f/r_i = 3.88$.

Figure 5 shows the result of a calculation in the Track Mode of ETrak with 40 model electrons. The particles start at a distance of 0.01 cm from the left-hand boundary with current assigned to

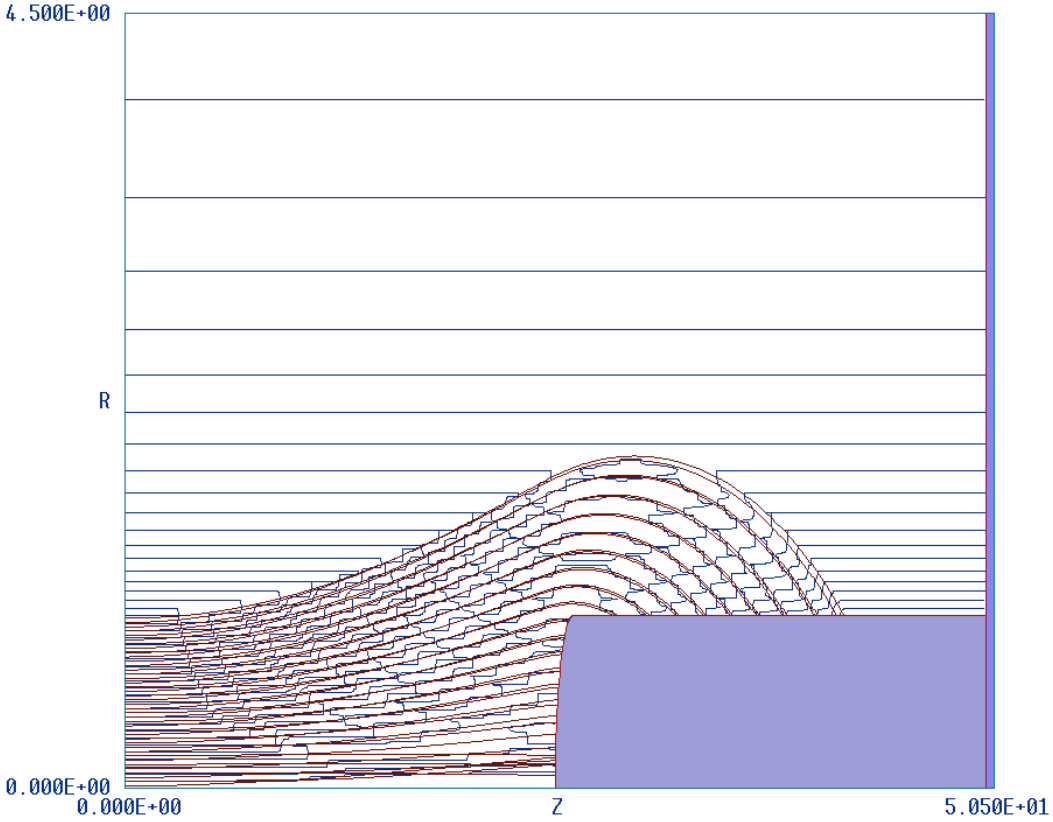

Figure 6a. Capture of an expanding relativistic beam (617.4 A, 1 MeV) by a grounded collector: electron orbits and lines of constant B_θ. Dimensions in cm, 10× vertical exaggeration. Collector volume shown in light blue.

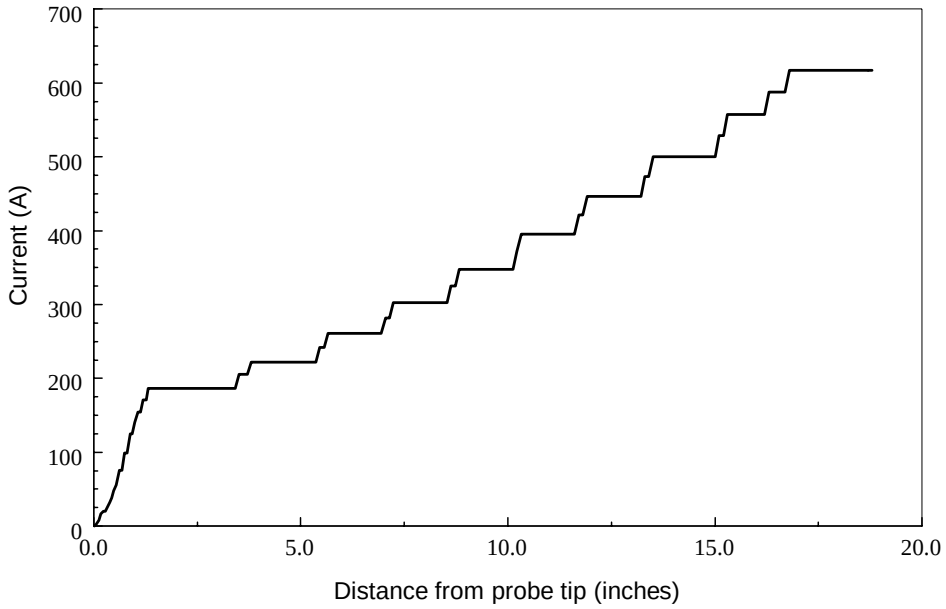

Figure 6b.Collected current as a function of distance from probe tip derived from face currents

approximate a uniform current density of j_z = 197 A/cm^2. The plots shows electron orbits and lines of constant B_θ. Note that there is a vertical magnification by a factor of 10. The vertices on the left-hand boundary share a Region Number and are specified as source points. The connected faces therefore have the Emission condition and program assigns the current of one or more particles with the closest starting point. Note that there is a thin target region along the right-hand boundary. It is treated as medium with $\varepsilon/\varepsilon_o - 1.0 \times 10^{-6}$ for the electrostatic calculation to preserve the Neumann boundary condition. The enclosed elements are designated as Material and the surfaces faces have the Collector characteristic. The presence of the layer ensures that electrons stop in a Material element. Linear interpolations are applied for both electric and magnetic forces. Note that the orbits are almost perfectly laminar and there is no sign of filamentation. The ratio of the final to initial envelope radius is 3.88. This is an absolute prediction with no adjustable parameters. The two imperfect orbits near the axis reflect a common problem in ray tracing codes. They result from accumulated interpolation errors in the region where two very small forces are balanced. The error in final position, 1 mm over 50 cm of transit, has a neglible effect on beam dynamics because the affected particles near axis carry only a small fraction of beam current. Contours of constant B_θ are also plotted in Fig. 5. The important point is that lines at large radius are parallel, even though the associated vertices connect to the axis along widely different logical paths. The effect demonstrates conservative of current in the propagation volume and along conducting boundaries.

Figure 6*a* shows a related example that would be difficult to handle with previous methods. Again, a 617.4 A 1 MeV electron beam expands from a waist with 1 cm radius. A grounded probe 25 cm downstream captures the beam. Note the probe has a spherical tip and that the plot has a 10× vertical exaggeration. Capture of the beam is a relativistic effect. The probe reduces the local radial electric field so that the beam magnetic force predominates. In the simulation is is essential to assign the current of impinging electrons to the front and side faces of the problem toderive the pinch force correctly. The parallelism of B_θ lines at large radius is a sensitiveindicatorof the validity of surface current assignment. The face-current method also provides useful diagnostic information. For example, we can make ordered list of face values to find the beam current distribution on the collector. Figure 6*b* shows collected current as a function of distance from the probe tip.

The simulation of Figure 7 illustrates assignment of initial electron parameters to represent space-charge-limited emission. Figure 7*a* and 7*b* show orbits and B_θ contours in a converging-beam gun for a relativistic klystron (420 A at 600 kV). The goal of the calculation is to get a good estimate of the current density distribution at the entrance to the transport region. The simulation is challenging because of substantial effects of the beam-generated magnetic field in the gun and transport regions, the complex electrode geometry, and the high beam convergence. The simulation employs a high-density mesh near axis to improve interpolations of the electric and magnetic forces. To smooth the current density distribution the calculation applies the ETrak capability to create multiple thermal electrons at initiation point. Five electrons with a transverse temperature of 1 eV start at each source location. The axial current density can be estimated at any point in the propagation volume by interpolations of B_θ at vertices. The code makes a radial scan of toroidal field and then takes numerical derivatives, $j_z = (1/\mu_0)\ (dB_\theta/dr + B_\theta/r)$. Fig. 7*c* shows resulting values for axial current density at the beam waist point in Fig. 7*a*.

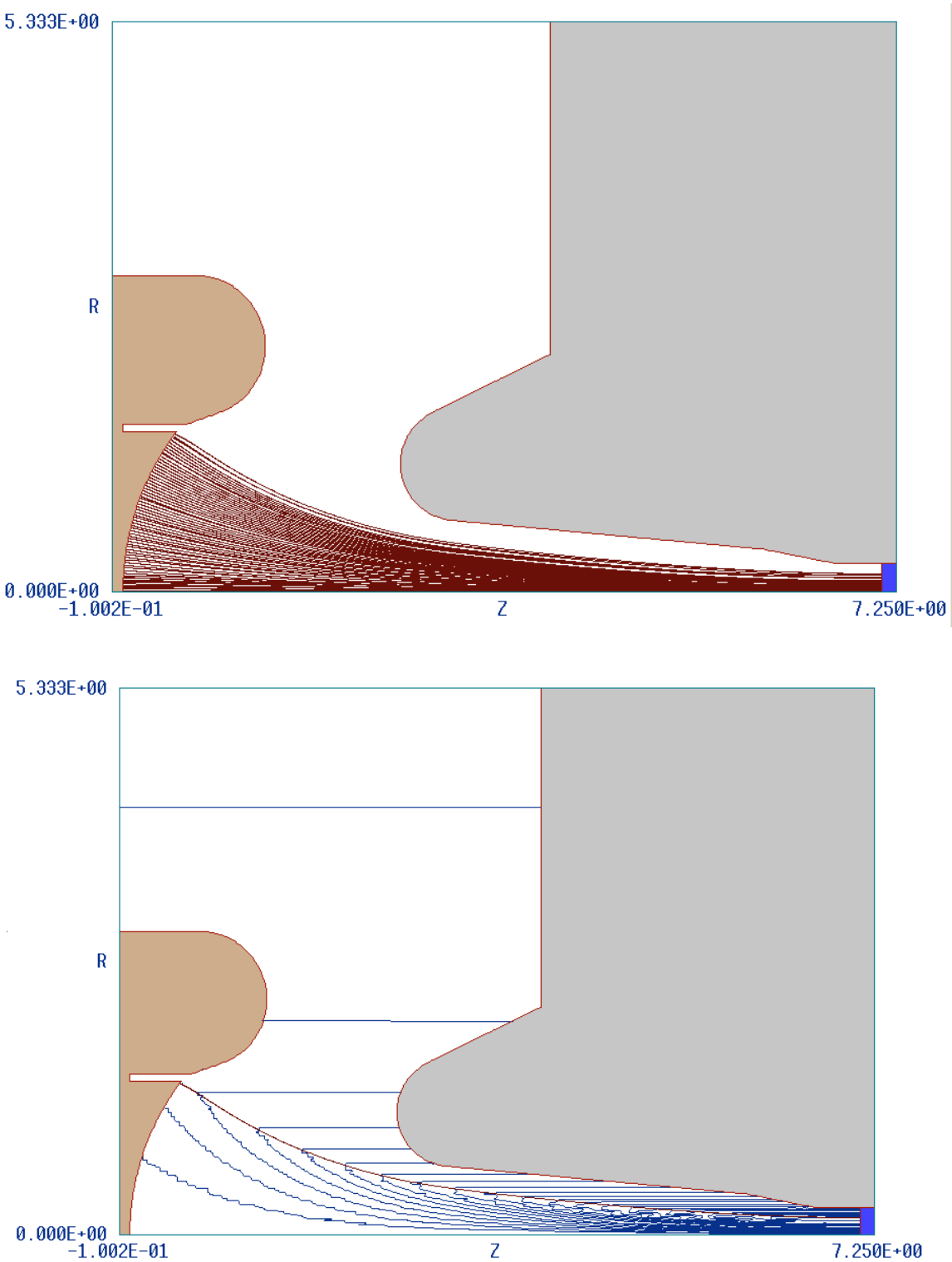

Figure 7. Relativistic electron gun, 420 A, 600 kV. Dimensions in inches. Top: Electron orbits. Bottom: Contours of constant B_θ.

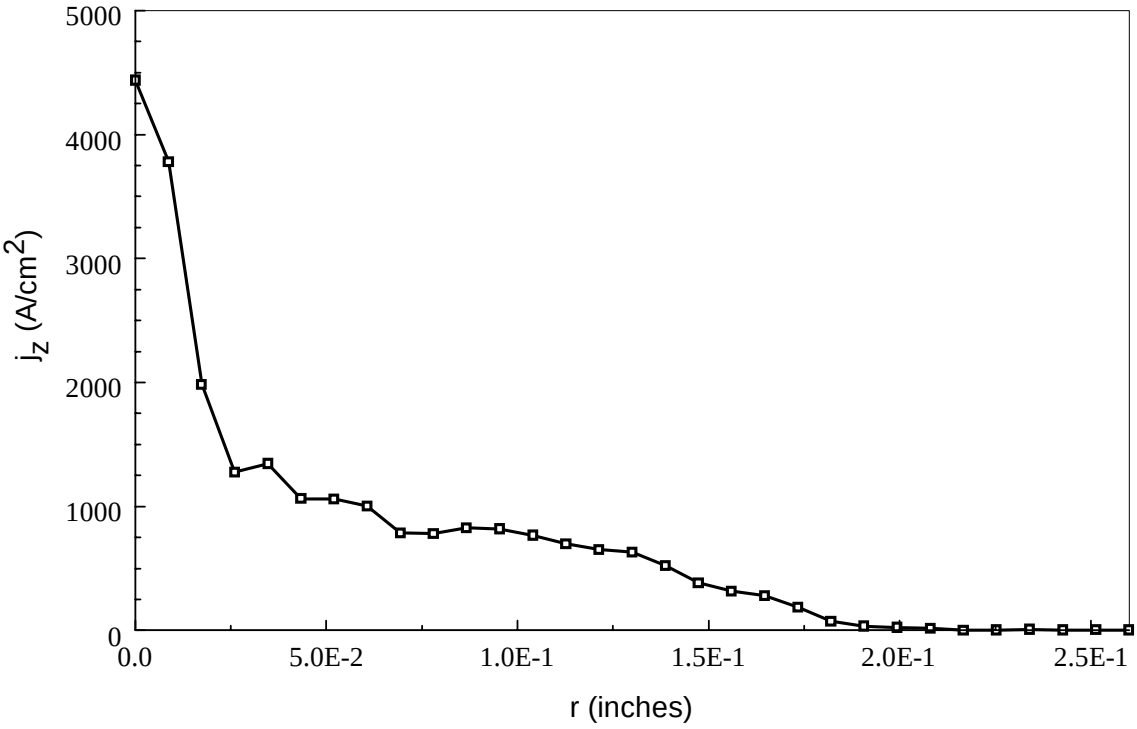

Figure 7c. Variation of current density at the point of maximum compression, derived from toroidal field information.

The final calculation of Fig. 8 utilizes all the techniques of the face-current method. The simulation addresses relativistic flow from a spherical cathode across a gap with 1 MV applied voltage. The collector and outer wall are grounded. Electrons are created on the cathode by explosive plasma emission with a surface temperature of 500 eV. The beam-generated magnetic field dominates electron behavior. It prevents radial electron flow, enhancing the space-charge density near the cathode and strongly influencing the total current. Some orbits travel backward and some return to the cathode, proving a rigourous test of current conservation. Note the parallelism of B_θ lines at large radius. These lines exhibit a noticeable slope if we deactivate the reassignment of relected electron current to Emission faces.

In conclusion, the face-current method gives physically-correct and accurate results, even for complicated gun geometries and reflex flows. We have shown that it can be implemented on a conformal triangle mesh. A significant advantage of the method is that it can be implemented automatically for most practical geometries with minimal user input.

This work was supported by Subcontract Number 4400000474 from Science Applications International Corporation under Contract Number N00014-97-C-2076 from the Naval Research Laboratory.

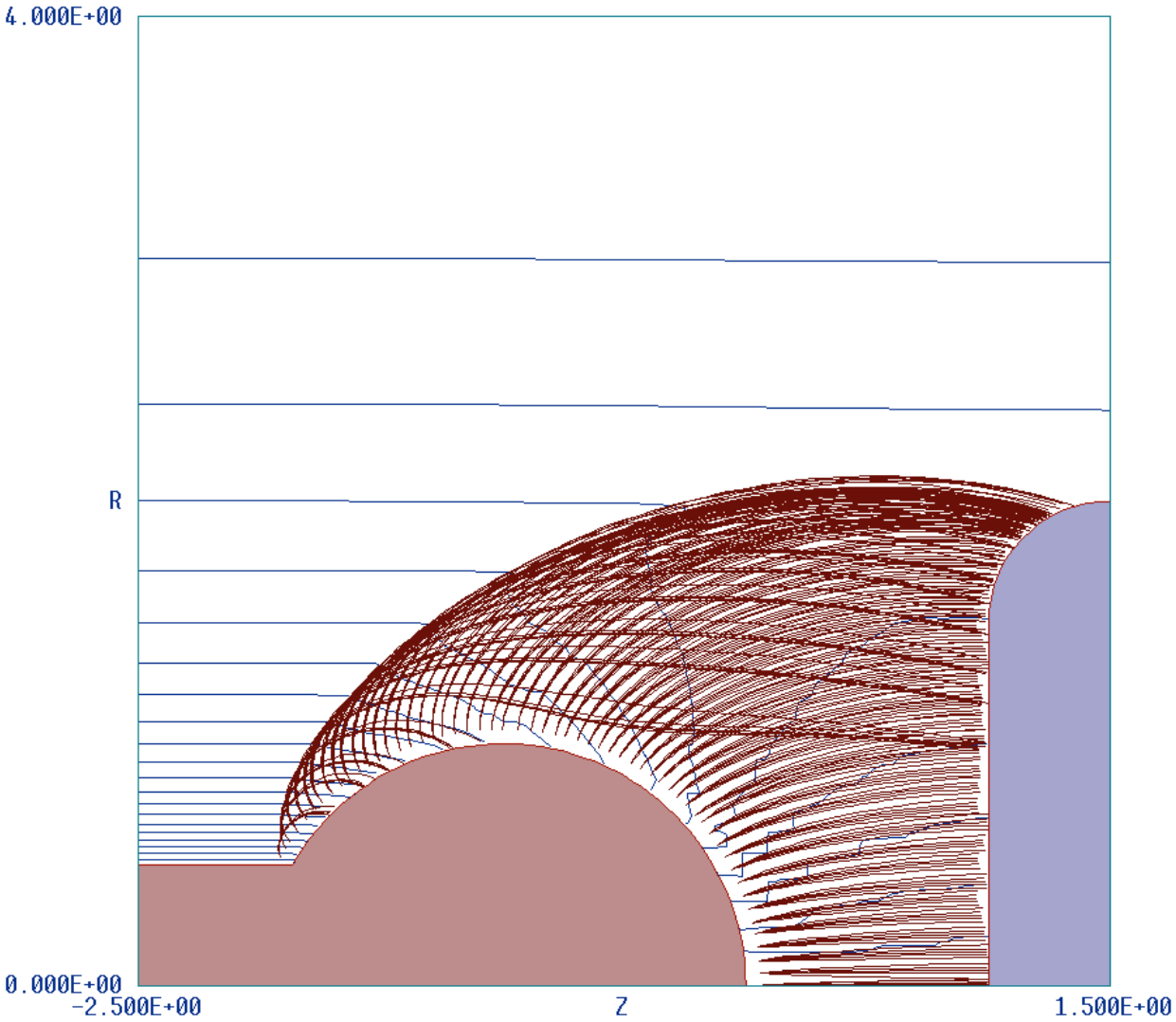

Figure 8. Relativistic flow from a spherical emitter.: 15.66 kA at 1 MeV. Dimensions in inches. Particles orbits and contours of constant B_0.

References

1. R. True, IEEE Trans. Nucl. Sci. **NS-32**, 2611 (1985).
2. *General Purpose Relativistic Beam Dynamics Code* in **Computational Accelerator Physics**, edited by R. Ryne (Am. Inst. of Physics, New York, 1994), 493.
3. *TRAK - Charged Particle Tracking in Electric and Magnetic Fields*, in **Computational Accelerator Physics** edited by R. Ryne (American Institute of Physics, New York, 1994), 597.
4. S. Humphries, Jr., J. Comp. Physics **125**, 488 (1996).
5. N.J. Dionne and H.J. Krahn (Raytheon Company, PT5599, 1980), unpublished.
6. W.B. Herrmannsfeldt (Stanford Linear Accelerator Center, SLAC-331, 1988), unpublished.
7. A.C. Paul (Lawrence Berkeley Laboratory, LBL-13241, 1982), unpublished.
8. D.L. Vogel (Lawrence Berkeley Laboratory, LBL-18871, 1985), unpublished.
9. J.E. Boers (Sandia National Laboratory, SAND 79-1027, 1980), unpublished.
10. See, for instance, S. Humphries, Jr., **Charged Particle Beams** (Wiley, New York, 1990), Sect. 7.3.
11. S. Humphries, Jr., J. Petillo and N. Dionne, *Secondary Electron Emission Models for Charged-particle Simulations on a Conformal Triangular Mesh*, submitted for publication.
12. See, for instance, S. Humphries, Jr., **Field Solutions on Computers** (CRC Press, Boca Raton, 1997), 71.
13. See, for instance, S. Humphries, Jr., **Charged Particle Beams** (Wiley, New York, 1990), Chap. 5.